Electronic Supplementary Material (ESI) for Catalysis Science & Technology.

Supporting information for

Group 13 metals doped Cu/ZnO catalysts from phase pure precursors via isomorphous substitution route: mechanistic insights on promotional effect for syngas hydrogenation to methanol

Nilesh Narkhede, Huayan Zheng, Huacheng Zhang, Guoqiang Zhang, Zhong Li **

Key Laboratory of Coal Science and Technology of Ministry of Education and Shanxi Province, Taiyuan University of Technology, Taiyuan 030024, Shanxi, China, *E-mail: zhenghuayan@tyut.edu.cn; lizhong@tyut.edu.cn

Contents **Page No.**

SI 01. Characterization techniques.

The N_2 adsorption-desorption measurements were performed on a Beishide 3H-2000PS2 apparatus at -196 °C after outgassing the samples under vacuum at 250 °C for 4 h. The specific surface area of the samples was calculated by the Brunauer-Emmett-Teller (BET) method, and the pore size distribution was measured using the Barrett-Joyner-Halenda (BJH) model.

The X-ray photoelectron spectroscopy (XPS) data was collected on an ESCALab220i-XL electron spectrometer (VG, UK) using 300 W AlKa radiation. The samples were compressed into a pellet of 2 mm thickness and then mounted on a sample holder by utilizing double-sided adhesive tape for XPS analysis. The sample holder was then placed into a fast entry air load-lock chamber without exposure to air and evacuated under vacuum ($<10^{-6}$ Torr) over night. Finally, the sample holder was transferred to the analysis chamber for XPS study. The base pressure inside the analysis chamber was usually maintained at better than 10^{-10} Torr. The C1s line (284.6 eV) was taken as a reference to correct for electrostatic charging.

The X-ray diffraction (XRD) measurements were performed on a Rigaku SmartLab SE X-ray diffractometer with CuKα radiation (40 kV, 40 mA). The patterns were recorded in steps of 0.01° with the scanning rate at 10°/min from 5° to 80° under atmospheric pressure.

The temperature-programmed reduction (TPR) experiments were carried out on Micromeritics AutoChem II 2920 equipment. Typically, 25 mg of catalyst was loaded into a U-shape quartz autoclave, and sample was degasified with argon (20 mL/min) at 200 °C for 2 h to remove physisorbed moisture. After cooling to room temperature, the gas was switched to 10% H_2 in argon flow (20 mL/min), and the temperature rose from 50 to 900 °C with a heating rate of 10 °C /min. Effluent gas was passed through a cold trap to trap moisture in effluent gas before reaching the thermal conductivity detector (TCD).

The % dispersion of Cu (D_{Cu}) and the exposed copper surface area (SA_{Cu}) were determined by dissociative N_2O adsorption and carried out on Micromeritics AutoChem II 2920 instrument. Firstly, the fresh catalysts (100 mg) were reduced by 10% H_2/Ar mixture until 450 °C is attained and the amount of hydrogen consumption was denoted as X. Then the reactor was then purged with N_2 and cooled to 50 °C. The N_2O gas was used to re-oxidized surface copper atoms to Cu_2O. Finally, a pulse of pure H_2 was passed over the catalyst and the surface Cu^+ were reduced in the pulse of pure H_2 and the amount of consumed H_2 was denoted as Y. By quantifying the amount of consumed H_2, the dispersion of Cu and exposed Cu surface area of the catalyst were calculated by Eq. (1) and Eq. (2) respectively.

$$D_{Cu} = \frac{2Y}{X} \times 100\% \quad (1)$$

$$SA_{Cu} = (2n_{H_2} \times N)/(1.4 \times 10^{19} \times W)\ (\mathrm{m^2/g}) \quad (2)$$

Where, D_{Cu} is dispersion of Cu, SA_{Cu} is surface area of Cu, n_{H_2} is the moles of consumed H_2, W is the weight of the catalyst, N is Avogadro's constant (6.02×10^{23} atoms mol^{-1}), and 1.4×10^{19} is the number of Cu atoms per square meter.

The ^{27}Al solid-state NMR spectra were recorded on a Bruker Avance II 300 spectrometer operating at 7.05 T with a resonance frequency of 78.2 MHz using a 4 mm triple-resonance magic-angle-spinning (MAS) probe and $AlCl_3$ as standard.

In situ DRIFTs spectra were collected on a Bruker EQUINOX55 FTIR spectrometer. Firstly, the catalyst was reduced under a H_2/Ar gas mixture (10 mL/min H_2 and 20 mL/min Ar) at 250°C for 90 min and subsequently sample was cooled down to room temperature. The sample was flushed with N_2 for 30 min to remove the residual H_2. After that, the reaction gas CO+H_2 (8.7 mL/min CO & 17.3 mL/min H_2) was passed through the sample for 10 min. The background spectrum was obtained at room temperature and the *in-situ* DRIFTs spectra were collected while increasing the sample temperature from room temperature to 300°C at a ramp rate of 5°C/min. The subsequent DRIFT spectra were obtained by subtracting the spectra obtained at 30°C, 50°C, 100°C, 150°C, 200°C, 250°C and 300°C by the background spectrum obtained at RT.

SI 02. Activity measurements.

The activity assessment of the catalysts was carried out on the continuous two-channel high-pressure fixed-bed microreactor (Xiamen Betterwork Intelligent Technology Co., Ltd.). A 200 mg of the calcined catalyst (40-60 mesh) was mixed with 200 mg of spherical quartz silica (40-60 mesh, 200 mg) in a central constant temperature zone of a (5 mm internal diameter) quartz tube reactor. Firstly, a mixture of H_2 and N_2 ($V_{H_2}:V_{N_2} = 1:4$) was introduced in the reactor at the total flow rate of 100 mL/min, then the temperature was raised to 250 °C at 2 °C /min and kept for 4 h for the reduction process. After naturally cooling down to 50 °C, the gas flow was switched from reducing gas to syngas ($V_{H_2}:V_{CO}:V_{CO_2}:V_{Ar} = 17.3:6.3:2.1:0.3$), the total gas flow was kept at 26 mL/min. Here, Ar was used as an internal standard. After the line was rinsed for 30 min, the unit pressure was slowly raised to 3 MPa, and the reaction temperature was raised to 250 °C at 2 °C/min to start the reaction. The gas composition after the reaction was analyzed by online gas chromatography (GC, Shanghai Haixin Chromatography Instrument Co., Ltd., model GC-950). The reactor to GC connection lines were kept at 120 °C to avoid condensation of the product. The GC was equipped with a TCD and FID detectors. Among them, the TCD detector was connected to the packed column, the column length was 1 m, the packing material was TDX-01 molecular sieve (supplied by Tianjin Chemical Reagent Co., Ltd.); the FID detector was connected to the capillary column, DB-624 UI (30m×0.32mm×1.80μm). After every 15 minutes, the outcoming gas mixture from the reactor was analyzed by GC in order to record the performance of the catalyst. The yield of methanol was calculated by the internal standard method based on the sum of the conversion rates of CO and CO_2 which were calculated by the change of CO/Ar and CO_2/Ar ratio before and after the reaction. The specific calculation formulas are given in equation (1) and (2).

$$X_{CO} = \frac{\left(\frac{CO_{feed}}{Ar_{feed}} - \frac{CO_{reaction}}{Ar_{reaction}}\right)}{\frac{CO_{feed}}{Ar_{feed}}} \qquad (1)$$

$$X_{CO_2} = \frac{\left(\frac{CO_{2feed}}{Ar_{feed}} - \frac{CO_{2reaction}}{Ar_{reaction}}\right)}{\frac{CO_{2feed}}{Ar_{feed}}} \qquad (2)$$

Where, X_{CO} and X_{CO_2} represent the conversion rates of CO and CO_2, respectively. CO_{feed}, $CO_{2_{feed}}$ and Ar_{feed} are the peak areas of the respective gases in the chromatogram before the catalytic reaction. The $CO_{reaction}$, $CO_{2_{reaction}}$ and $Ar_{reaction}$ are the corresponding peak areas of the gases in the chromatogram during the reaction. The methanol yield was calculated from the molar flow rates of CO and CO_2 as given in equation (3) and (4). The TOFs were calculated by using equation (5).

$$STY_{MeOH} = X_{CO} \times n_{co} + X_{CO_2} \times n_{CO_2} \qquad (3)$$

$$n_{CO} = \frac{Q_{CO} \times P}{RT} \times \varphi \quad \text{and} \quad n_{CO_2} = \frac{Q_{CO_2} \times P}{RT} \times \varphi \quad (4)$$

Where, STY_{MeOH} represents the yield of methanol; n_{CO} and n_{CO_2} represent the molar flow rates of CO and CO_2, respectively; Q_{CO} and Q_{CO_2} represent the mole fraction of CO and CO_2 in the feed; P and T represent the calibration pressure of the mass flow controller and temperature, respectively; φ represents the total flow rate of the intake gases.

$$TOF = \frac{F_{CO} \times CO\ conversion}{1000 \times V_m \times n_{Cu}} (min^{-1}) \qquad (5)$$

Where, F_{CO} is the CO flow rate (mL/min), V_m is the molar volume of the ideal gas at 25°C (24.5 L/mol) and n_{Cu} is the exposed Cu atoms of the loaded catalysts for the catalytic test determined from N_2O chemisorption.

SI 03. Zinc coverage (θ_{Zn}) measurements.

A 100 mg of catalyst (CZ-C, CZ-R, CZ/Al-C and CZ/Al-R) was subjected to H_2 pretreatment (10% H_2/Ar) at the flow rate of 40 mL/min and the temperature was increased to 220 °C at 10 °C/min and hold for 1 h. This followed by H_2 desorption at 450°C at 10°C/min. After cooling down to 60°C, N_2O was introduced and hold for 1 h to oxidize the Cu surface before the H_2-TPD measurements. The overall sequence of treatments is shown in Scheme S1. The Zn coverage, θ_{Zn} was estimated by following equation (6) reported by Sehested, et al.[1] using H_2 desorption capacity.

$$\theta_{Zn} = \frac{\eta_{H_2-STD}/0.96-\eta_{H_2-TPD}}{\eta_{H_2-STD}/0.96} \qquad (6)$$

Where, η_{H_2-STD} is the hydrogen desorption capacity of the catalysts without syngas treatment and η_{H_2-TPD} is the hydrogen desorption capacity after syngas treatment.

Scheme S1. Schematic depiction of the experimental processes applied for measurements of θ_{Zn}.

SI 04. XRD spectra of controls and CZ/Al$_x$ precursors.

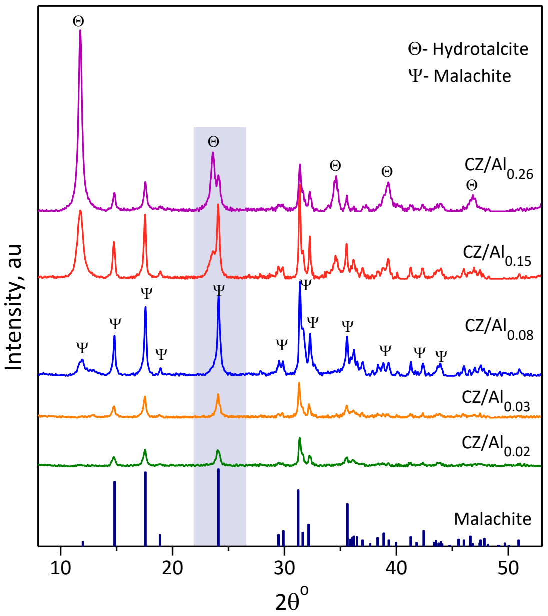

Fig. S1. XRD of the catalyst precursors, CZ/Al$_x$ (where, x = Al/(Al+Cu)) prepared via IS method (Malachite: JCPDS #41-1390).

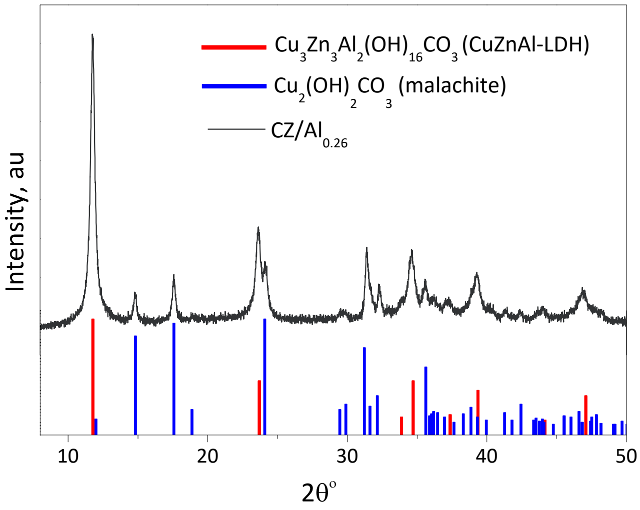

Fig S2. XRD pattern of CZ/$Al_{0.26}$ precursor prepared by IS method. (CuZnAl-LDH: JCPDS#37-0629 and Malachite: JCPDS #41-1390).

SI 05. Synthesis scheme for CZ/M-C catalysts by using IS method.

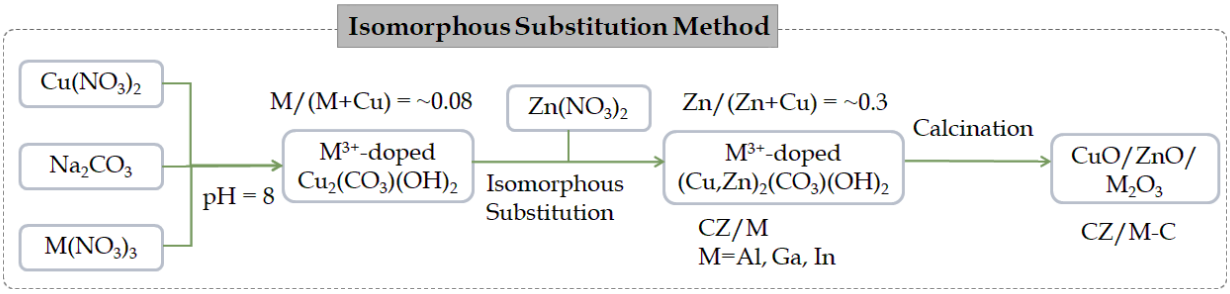

Fig. S3. Schematic representation of synthesis of CZ/M-C catalysts using IS method.

SI 06. Rietveld fit of the CZ/Al precursor.

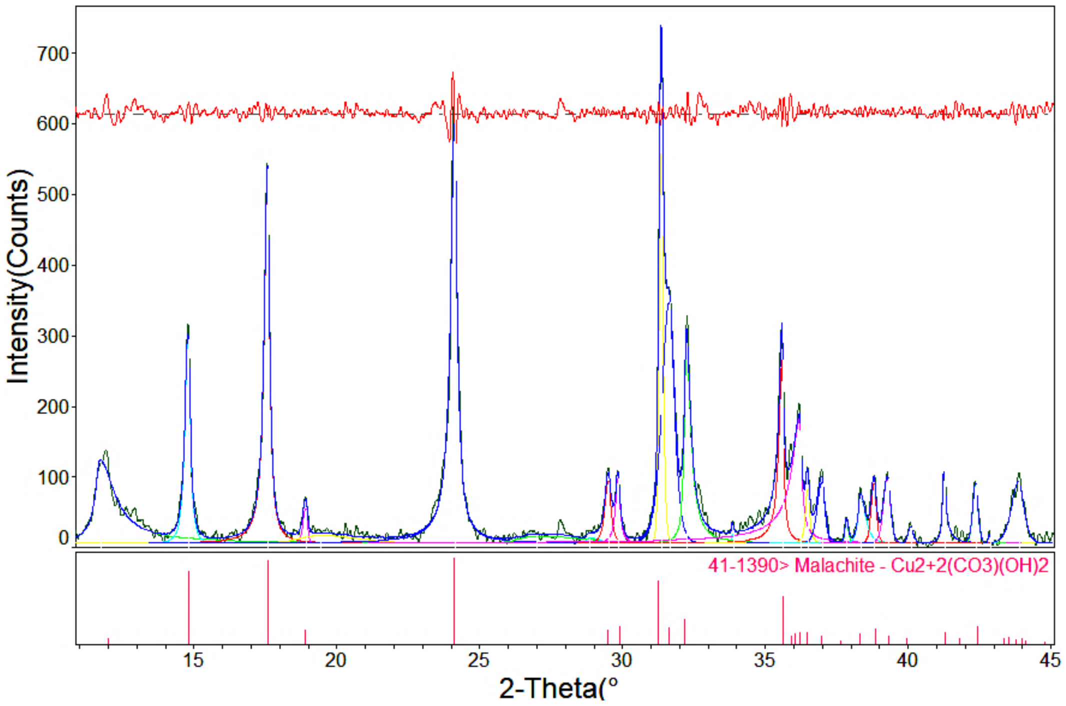

Fig. S4. Representative Rietveld fit of the CZ/Al precursor. (colour codes: experimental data: green; calculated pattern: blue; difference curve: red).

SI 07. HR-TEM and STEM-EDS images of CZ/M-C.

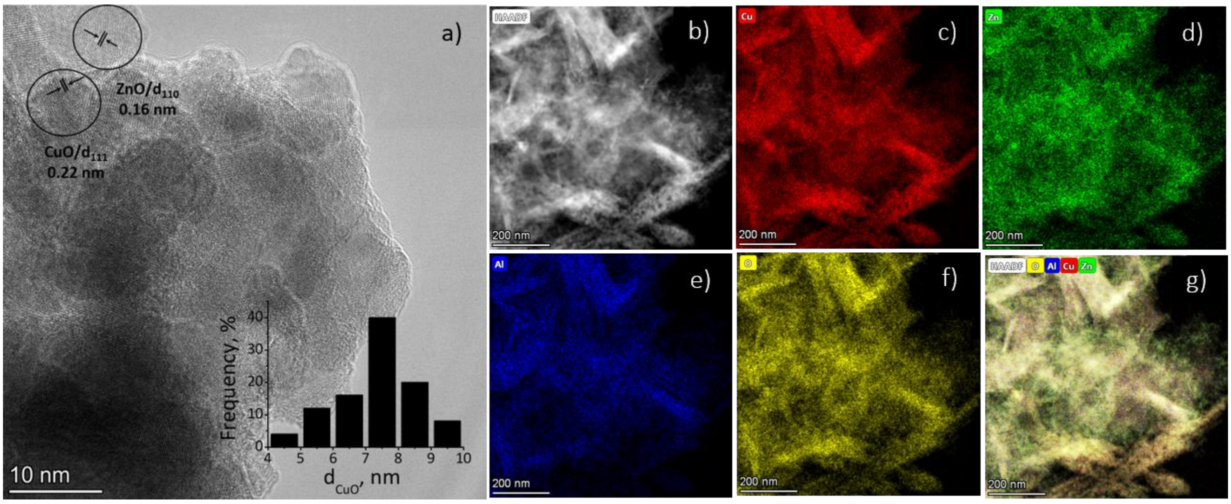

Fig. S5. (a) HR-TEM image (inset: particle size distribution) and (b-g) EDX elemental maps obtained in STEM-HAADF mode for oxide catalyst, CZ/Al-C (Colour code: Cu = red, Zn = green, Al = blue and O = yellow).

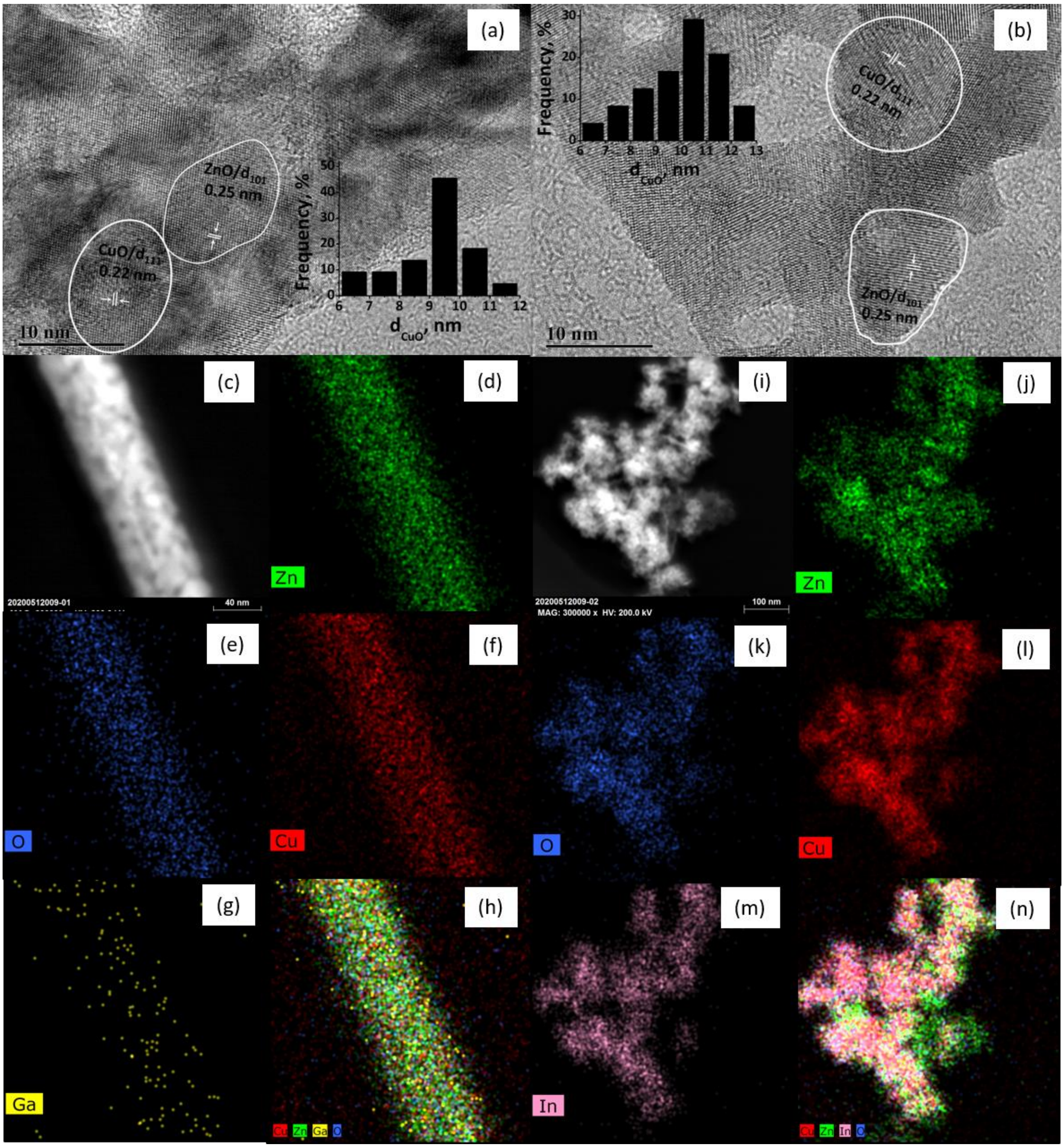

Fig. S6. HR-TEM images and particle size distribution of CuO domains (inset) of (a) CZ/Ga-C and (b) CZ/In-C. STEM-EDX elemental maps for (c-h) CZ/Ga-C and (i-n) CZ/In-C.

SI 08. *In-situ* Powder XRD analysis.

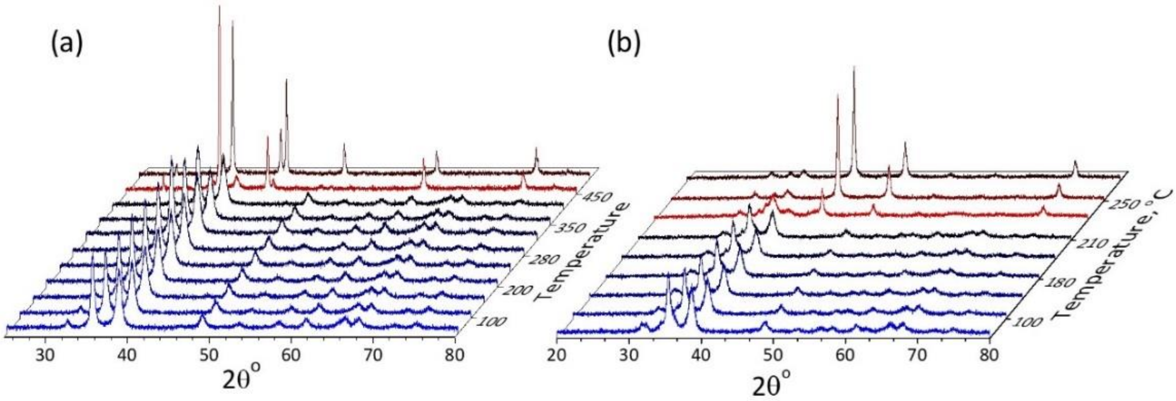

Fig. S7. Powder XRD patterns. *In-situ* reduction of (a) pure CuO (prepared from malachite) and (b) CZ-C under H_2/Ar = 10%.

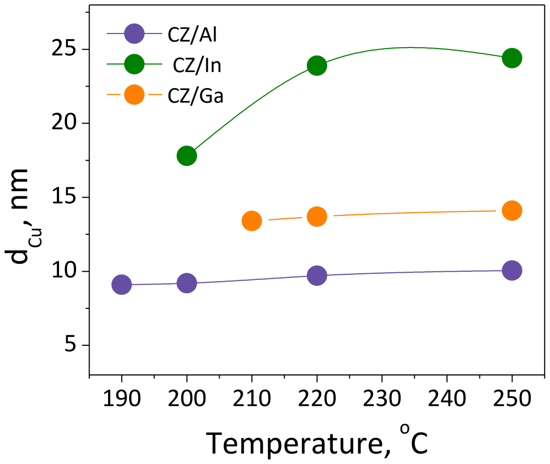

Fig. S8. Crystallite size of Cu^0 domains obtained from in situ XRD measurements of M^{3+}-doped catalysts.

SI 09. Crystallite size of Cu domains of the spent catalysts.

Table S1. The crystallite size of Cu domains for spent CZ/M-R catalysts.

Catalyst	Crystallite Size, nm	
	$^{a}d_{Cu}$	$^{b}d_{CuO}$
CZ-R	56.1	-
CZ/Al-R	10.1	-
CZ/Ga-R	21.4	13.2
CZ/In-R	40.7	-

Crystallite size calculated by using Scherrer formula at $2\theta = {}^{a}43.2$ *for* Cu^0 *and* ${}^{b}35.5$ *for CuO.*

SI 10. Rietveld fit of the spent catalysts.

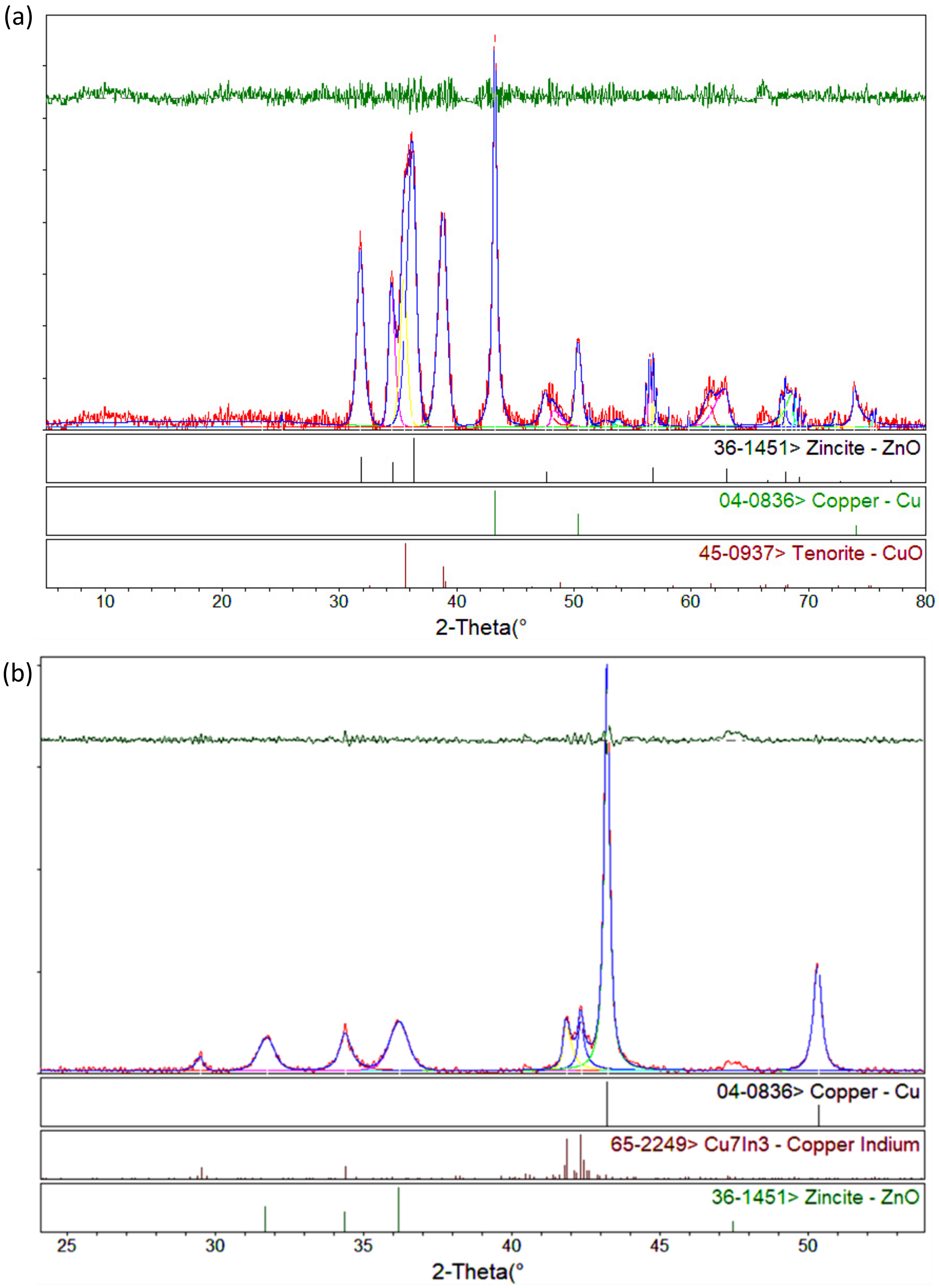

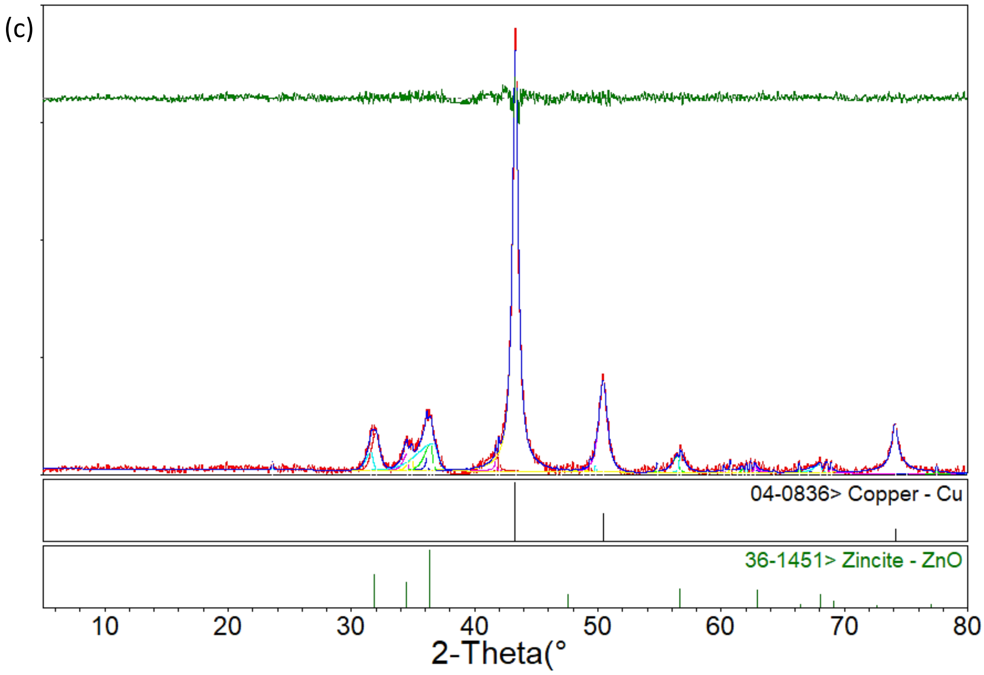

Fig. S9. Rietveld fit of the spent (a) CZ/Ga-R, (b) CZ/In-R and (c) CZ/Al-R catalysts.

SI 11. Zn LMM AES spectra of Ga^{3+} and In^{3+}-doped spent catalysts.

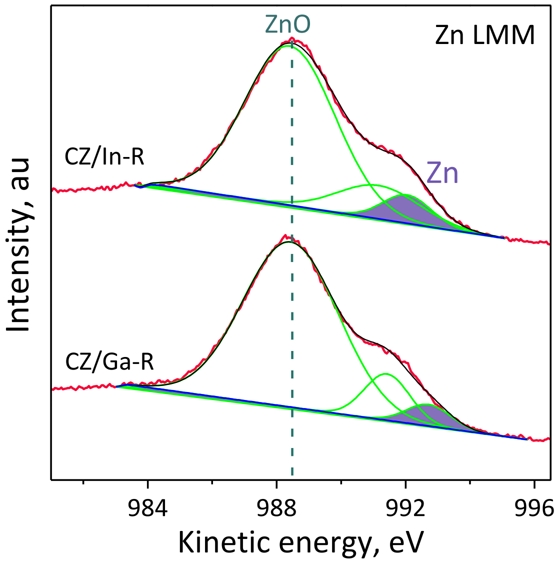

Fig. S10. Zn LMM AES spectra of Ga^{3+} and In^{3+}-doped spent catalysts. Where, dark shaded region represents reduced Zn, red lines are the AES data-set and black lines stand for the best fit of AES data.

SI 12. H_2 and CO TPD data of pre-reduced catalysts.

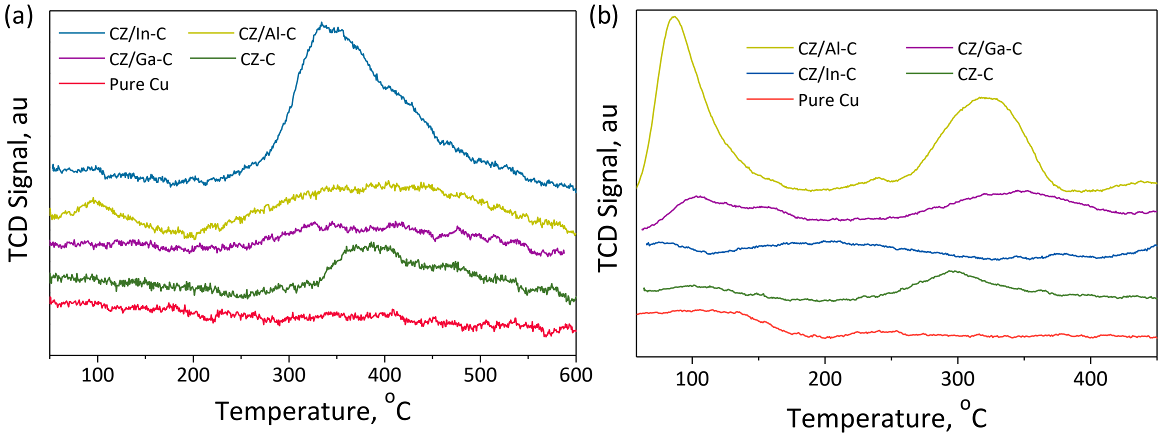

Fig. S11. (a) H_2 TPD and (b) CO TPD profiles of pre-reduced CZ/M-C ($Cu/ZnO/M_2O_3$), CZ-C (Cu/ZnO) and pure Cu. (Pure Cu was prepared from pure phase $Cu_2(OH)_2CO_3$).

The H_2-TPD results (Fig. S11a) suggest that negligible amount of H_2 has been desorbed from pure Cu while, the binary catalyst show significant H_2 desorption at ~386°C. This high temperature desorption is usually related to spillover H atoms which are dissociated from Cu surface to the ZnO surface at the Cu-ZnO interface.[2] The incorporation of Al_2O_3 exhibits presence of a low temperature peak (~95°C) due to the desorption of weakly bound hydrogen. Further, the high temperature hydrogen desorption peak is broadened with 2-fold increase in the amount of H_2 desorbed as compared to the binary Cu/ZnO system suggesting the increased spillover effect upon Al^{3+} incorporation. The In^{3+}-doped catalyst showed exceptionally high H_2 desorption at higher temperature (Table S2). The results supported the fact that introduction of promoters increases the adsorption sites of the spillover hydrogen in the catalyst which is conductive for the methanol formation.

The CO TPD profiles of the M^{3+}-doped catalysts along with the controls are given in Fig. S11b and the corresponding data are given in supporting information Table S2. It is apparent that, the overall CO adsorption capacity of Cu/ZnO based catalyst, CZ-C was increased by 2-fold as compared to the pure Cu alone. Further, the addition of Ga^{3+} and In^{3+} leads to a small increase in the CO adsorption capacity however, that for the Al^{3+} doped catalyst was increased by ~5.5 fold as compared to the binary Cu/ZnO catalyst. The increased intensity of the α peak for CZ/Al-C suggests that, below reaction temperature (<250°C) maximum CO has been adsorbed on the Al_2O_3 surface during methanol synthesis. The promoter induced oxygen vacancies are supposed to be responsible for CO adsorption and activation for subsequent hydrogenation reaction.[3]

Table S2. CO-TPD and H_2-TPD data of controls and CZ/M-C.

Sample	CO TPD				H_2 TPD			
	Peak α		Peak β		Peak α		Peak β	
	T°C	Q, mmol/g	T°C	Q, mmol/g	T°C	Q, μmol/g	T°C	Q, μmol/g
Pure Cu	134	0.027	240	0.011	180	1.145	414	6.215
CZ-C	113	0.011	294	0.062	218	1.452	386	32.777
CZ/In-C	211	0.049	373	0.004	-	-	334	83.745
CZ/Ga-C	103	0.054	344	0.065	120	2.316	326	26.517
CZ/Al-C	87	0.222	321	0.187	95	4.187	404	65.602

Q = CO or H_2 desorption quantity, Pure Cu = Cu prepared from pure phase $Cu_2(OH)_2CO_3$. Peak α = low temperature, Peak β = high temperature peak.

SI 13. DRIFT-IR spectra of CO+H_2 co-adsorption.

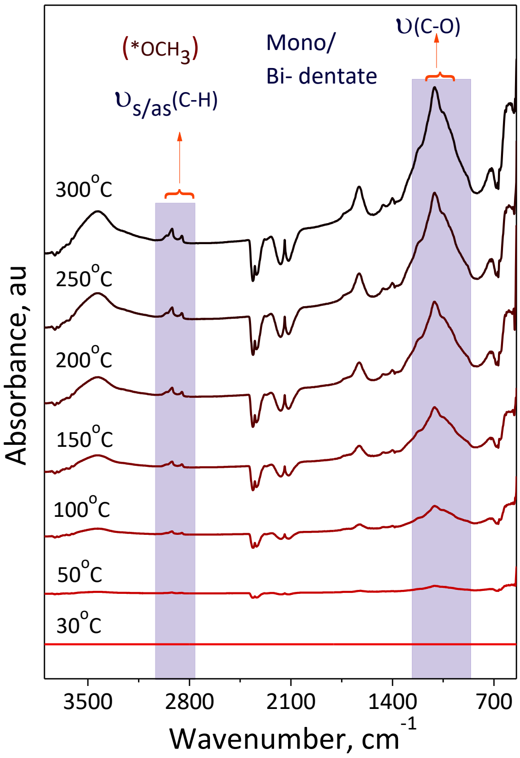

Fig. S12. DRIFT-IR difference spectra of CO+H_2 co-adsorption on the pre-reduced Al^{3+}-doped catalyst.

The DRIFT spectra for co-adsorption of CO+H_2 on the *in-situ* reduced catalyst, CZ/Al-R were obtained by background correction of the spectra at different temperatures with that at room temperature (Fig. S12). On increasing the temperature, the peaks at 1054 cm^{-1} (bidentate υ_{CO}) and 1107 cm^{-1} (monodentate υ_{CO}) for C-O stretch as well as at 2851 cm^{-1} (υ_{CH}), 2920 cm^{-1} (υ_{CH}) for C-H stretch of the -CH_3O group were increased predominantly.[4, 5] The formation of methoxy intermediate is visible beyond 150°C and the concentration of it was found to increase with the temperature. Further, the absence of bands corresponding to -HOCO and CO_3^{2-} supports the fact that methanol formation by CO+H_2 hydrogenation takes place via -OCH_3 intermediate. The formation of methanol from CO+H_2 is postulated to occur by step-wise reduction of CO through -CHO, -CH_2O and -CH_3O and the detected band corresponding to -CH_3O is the last intermediate to methanol formation. The methoxy group was further found to be attached to catalyst surface in bidentate manner.

SI 14. Comparison with catalysts prepared from state-of-the-art methods.

Table S3. Comparison of the microstructure properties and catalytic performance of the $Cu/ZnO/Al_2O_3$ catalysts for syngas hydrogenation to methanol.

Method	Al/ (Al+Cu)	SA_{BET}, m^2/g	SA_{Cu}, m^2/g	D_{Cu}, %	d_{CuO}, nm	P/T (MPa/°C)	STY_{MeOH}	Reference
CP	0.082	91	18.6	2.75	8.8	5/250	538	6
CP	0.084	127	41.5	14.4	16.2	5/250	463	7
CP	0.1	78	38.9	3.95	8.8	5/250	430	8
ICI	0.14	115	25	6.4	-	5/250	506	9
ICI	0.45	-	-	-	-	3/250	326	10
CP[a]	0.33	112.5	33.3	20.2	7.2	3/250	511	This work
IS	0.084	72	52	16.2	5.9	3/250	855	This work

[a] $Cu_{0.4}Zn_{0.4}Al_{0.2}$ prepared by coprecipitation method as described in reference 11. CP = coprecipitation, IS= isomorphous substitution, ICI = Imperial Chemical Industries proprietary procedure, SA= surface area, D_{Cu} = % Cu dispersion, d_{CuO} = CuO crystallite size, STY_{MeOH} *in $mg/g_{cat}/h$, P=reaction pressure, T= reaction temperature.*

New synthetic approaches are being established which can possibly substitute the benchmark “coprecipitation” (CP) route that does not offer controlled formation of pure phase hydroxycarbonates of Cu and Zn. However, it was difficult to accomplish better performance than that of Cu/ZnO catalyst prepared by state-of-the-art CP method. In order to demonstrate the superiority of the present synthetic strategy, the comparison of best performing catalyst, CZ/Al-C prepared by IS method with those prepared from state-of-the-art CP method has been summarized in brief in Table S3. It is evident that the present catalytic system demonstrates formation of $Cu/ZnO/Al_2O_3$ catalyst with improved Cu surface area, finest Cu dispersion and smaller particle size which are critical properties for excellent catalytic performance for syngas hydrogenation.

Further, in order show the competency of the present CZ/Al-C with the industrially used $Cu/ZnO/Al_2O_3$ catalyst under similar reaction condition, the catalyst, $Cu_{0.4}Zn_{0.4}Al_{0.2}$-CP was prepared by standard CP method and subjected to the methanol synthesis (Table S3). The catalyst, CZ/Al-C showed higher exposed Cu surface area and smaller particle size of CuO domains than $Cu_{0.4}Zn_{0.4}Al_{0.2}$-CP. This has resulted in ~1.7-fold higher STY_{MeOH} than that of $Cu_{0.4}Zn_{0.4}Al_{0.2}$-

CP. The superiority of the present catalyst system could be attributed to the excellent microstructure properties which are primarily related to the precursor chemistry of the present CZ/Al-C catalyst. The XRD pattern of the coprecipitated $Cu_{0.4}Zn_{0.4}Al_{0.2}$-CP precursor showed the presence of several constituent phases, viz., aurichalcite, malachite and hydrotalcite (Fig. S13) suggesting the formation of several metal hydroxy carbonate by-phases via CP method. These mixtures are difficult to characterize comprehensively owing to the varying Cu:Zn:Al ratios of the individual single phases and their typically low crystallinity. In addition to that, all the components of the precursor mixture can lead to various domains in the $Cu/ZnO/Al_2O_3$ catalysts with different types of materials with individual textural and catalytic properties. Together, these domains make up less active catalytic systems with inhomogeneous microstructures and lead to the catalyst deactivation via sintering of Cu species. Whereas, incorporation of Al^{3+} in zM via IS method caused maximum dilution of Cu that has resulted the CZ/Al-C catalyst with improved physicochemical properties that represent critical structural features for better catalytic performance. These metal oxides are known to persist the chemical memories of the elements from their precursors to the calcined further to the reduced states. Hence, the phase-pure zM precursor with optimal Al^{3+} doping prepared by IS method exhibits a perfect atomic distribution of all the three metal components and elicit the homogeneous dispersion of all the constituent phases in the calcined catalyst that further stabilize the size and dispersion state of Cu in the reduced catalyst.

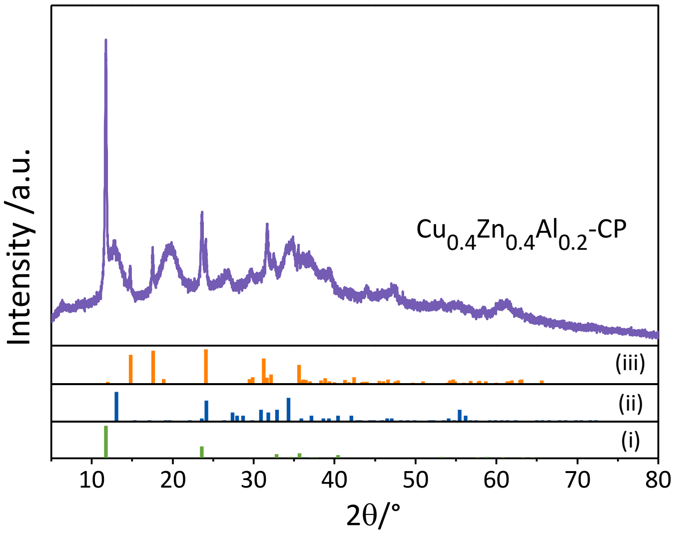

Fig. S13. XRD pattern of the $Cu_{0.4}Zn_{0.4}Al_{0.2}$-CP precursor prepared by CP method (where, i, ii and iii are standards for Cu-Al hydrotalcite (JCPDS#37-0630), aurichalcite (JCPDS#17-0743) and malachite (JCPDS#41-1309), respectively).

References

1. S. Kuld, M. Thorhauge, H. Falsig, C. F. Elkjær, S. Helveg, I. Chorkendorff and J. Sehested, *Science*, 2016, **352**, 969-974.
2. S. Natesakhawat, P. R. Ohodnicki, B. H. Howard, J. W. Lekse, J. P. Baltrus and C. Matranga, *Top. Catal.*, 2013, **56**, 1752-1763.
3. L. Li, W. Li, C. Zhu and L.-F. Mao, *physica status solidi (b)*, 2019, **256**, 1800386.
4. L. G. A. van de Water, S. K. Wilkinson, R. A. P. Smith and M. J. Watson, *J. Catal.*, 2018, **364**, 57-68.
5. I. Abbas, H. Kim, C.-H. Shin, S. Yoon and K.-D. Jung, *Appl. Catal. B: Environ.*, 2019, **258**, 117971.
6. M. Sadeghinia, A. Nemati Kharat Ghaziani and M. Rezaei, *Mol. Catal.*, 2018, **456**, 38-48.
7. Q. Zhu, Q. Zhang and L. Wen, *Fuel Process. Technol.*, 2017, **156**, 280-289.
8. M. Sadeghinia, M. Rezaei, A. Nemati Kharat, M. Namayandeh Jorabchi, B. Nematollahi and F. Zareiekordshouli, *Mol. Catal.*, 2020, **484**, 110776.
9. M. Sahibzada, I. S. Metcalfe and D. Chadwick, *J. Catal.*, 1998, **174**, 111-118.
10. J. S. Lee, S. H. Han, H. G. Kim, K. H. Lee and Y. G. Kim, *Korean J. Chem. Eng.*, 2000, **17**, 332-336.
11. M. M. J. Li, C. Chen, T. Ayvalı, H. Suo, J. Zheng, I. F. Teixeira, L. Ye, H. Zou, D. O’Hare and S. C. E. Tsang, *ACS Catal.*, 2018, **8**, 4390-4401.